9TH INTERNATIONAL SYMPOSIUM ON FLOW VISUALISATION, 2000

STOCHASTIC MODELING AND SIMULATION OF TURBULENT REACTING FLOWS

S.C. Garrick[1], **V. Interante**[2]

Keywords: *Turbulence, Large Eddy Simulation, Feature Extraction, Volume Rendering, Isosurfaces.*

ABSTRACT

The filtered density function (FDF) is implemented for large eddy simulation of three-dimensional, planar jets under both non-reacting and chemically reacting conditions. In this methodology, the effects of the unresolved scalar fluctuations are taken into account by considering the joint probability density function of the scalar quantities in a stochastic manner. It is shown that under reacting flow conditions, the absence of closure for the SGS scalar correlations yields results which are significantly different from those obtained by the FDF. We visualize this data with a combination of volume and isosurface rendering, and introduce methods for reducing the memory and time costs that have historically precluded recording the results of the simulation at all calculated time steps.

1 INTRODUCTION

There are three general methods of implementing CFD for turbulence simulations [17]: Reynolds averaged Navier-Stokes simulation (RANS); large eddy simulation (LES); and direct numerical simulation (DNS). In RANS the solution of the "averaged" Navier-Stokes equations is attempted. This procedure is based on the original idea by Reynolds[32] who suggested the decomposition of the turbulence fields into instantaneous and fluctuating counterparts. While this approach may be adequate in capturing some of the overall mean flow features, time sensitive details of the flow would not be elucidated. This restricts the range of flows which can be studied. DNS involves the solution of the governing equations on a computational grid fine enough to resolve the Kolmogoroff scales[21]. Typically the number of grid points required for reliable simulation is proportional to $Re^{9/4}$, where Re is the characteristic Reynolds number. This spatial resolution, along with its corresponding temporal resolution, renders DNS prohibitively expensive [11]. Large eddy simulation (LES) facilitates the solution of the spatially (and/or temporally) filtered governing equations [16, 1, 10, 9]. The transport variables are decomposed into the resolved grid scale and the unresolved or sub-grid scale (SGS) quantities. A SGS closure is needed to prescribe the non-linear interactions between the large (resolved) scales and the small (unresolved) scales in terms of resolved scale quantities only. The presence of chemical reactions introduces additional interactions, both scalar-scalar and hydro-scalar, which need to be accounted for. In the

Author(s): [1]*Department of Mechanical Engineering, University of Minnesota, Minneapolis, MN, USA.*
[2]*Department of Computer Science and Engineering University of Minnesota, Minneapolis, MN, USA.*

Corresponding author: garrick@me.umn.edu

context of RANS it is now widely recognized that these fluctuations are important[22, 20, 18]. Significant progress has been made with the approach based on probability density functions (PDFs)[28, 27, 24]. With the knowledge of the joint PDF of the scalars, the effect of chemical reaction on scalar transport is taken into account exactly. This approach has been extended to LES in the form of the filtered density function (FDF)[26, 12, 6, 5, 19, 15].

The basic element of the FDF methodology is the accounting for the effects of unresolved quantities in a stochastic manner. Such an approach has widespread application in both premixed and non-premixed combustion. In these applications, fuel and oxidizer are introduced, mix, and react. However, because of mixing and varying hydro-chemical conditions, combustion systems are susceptible to such things as flashback, auto-ignition, and pre-detonation. Such highly time-dependent, hydro-chemical phenomena, which are currently beyond the reach of RANS, are fully resolvable using the FDF methodology. The FDF greatly reduces the computational cost associated with the numerical simulation of turbulent reacting flows such as those found in internal combustion engines, gas turbines, industrial furnaces, and other engineering applications.

A number of challenges are faced in effectively visualizing the large amounts of data that are produced in these calculations. The most critical of these is to define a method for automatically detecting, extracting, and efficiently storing for further processing the specific features of interest. Because of the sheer quantity of data produced, it is infeasible to follow a strategy in which all of the data is first stored, and then subsequently processed for visualization. The time that would be required to simply write all of the data to disk would slow the calculations from days to weeks. The key to the strategy that we employ is to recognize that in these terabytes of data, there is actually only a small subset that is truly of scientific interest. By extracting and saving only the subset of each volume, at each time step, which gives the most directly relevant insights into the processes under investigation, we can reduce the amount of data that needs to be visualized, both simplifying and improving the visualization process by more effectively conveying the most important information while minimizing or eliminating the extraneous detail.

The issue of primary concern is to assess the performance of the FDF and to appraise its generality and extent of predictive capability, by its application to a wider range of flows. In doing so we examine hydro-chemical structures using advanced data visualization algorithms not only as a post-process, but also in an *in situ* manner, thus facilitating the investigation of highly transient flow physics.

2 FORMULATION

2.1 Governing Equations

The flows under consideration are incompressible, turbulent, reacting jets involving N_s species. The primary variables are the velocity vector $u_i(\mathbf{x},t)(i=1,2,3)$, the fluid pressure $p(\mathbf{x},t)$, and the species mass fractions $\phi_\alpha(\mathbf{x},t)(\alpha=1,2,...,N_s)$. In addition to the conservation of mass and momentum equations, a set of species conservation equations are solved:

$$\frac{\partial \phi_\alpha}{\partial t} + \frac{\partial \phi_\alpha u_j}{\partial x_j} = -\frac{\partial J_j{}^\alpha}{\partial x_j} + \omega_\alpha, \tag{1}$$

The chemical source term is represented by ω_α and utilizing the Fickian diffusion assumption the scalar flux is given by $J_j^\alpha = -\Gamma \frac{\partial \phi_\alpha}{\partial x_j}$, where $\Gamma = \frac{\mu}{\rho Sc}$ is the molecular diffusivity and Sc is the molecular Schmidt Number. In LES, the filtering is accomplished by passing the flow variables through a convolution filter,

$$\langle \phi(\underline{x},t)\rangle_L = \int_{-\infty}^{\infty} h_s(\underline{x}-\underline{x}')\phi(\underline{x}',t), d\underline{x}' \tag{2}$$

where $\phi(\underline{x},t)$ is the variable being filtered, $h_s(\underline{x})$ is an isotropic, non-negative definite, spatial filter, and $\langle\phi(\underline{x},t)\rangle_L$ is the variable with the high wavenumber content removed.

The large scale component, or the "mean," is associated with the size of the filter, Δ, which is typically taken as some multiple of the computational mesh size. The ideal value for Δ is one lying just outside of the energy containing range of the spectrum [1]. Applying the filter to the governing equations yields:

$$\frac{\partial\langle u_j\rangle_L}{\partial x_j} = 0 \tag{3}$$

$$\frac{\partial\langle u_i\rangle_L}{\partial t} + \frac{\partial\langle u_i\rangle_L\langle u_j\rangle_L}{\partial x_j} = -\frac{\partial\langle p\rangle_L}{\partial x_i} + \frac{\partial\langle\tau_{ij}\rangle_L}{\partial x_j} - \frac{\partial T_{ij}}{\partial x_j} \tag{4}$$

$$\frac{\partial\langle\phi_\alpha\rangle_L}{\partial t} + \frac{\partial\langle u_j\rangle_L\langle\phi_\alpha\rangle_L}{\partial x_j} = -\frac{\partial\langle J_i^\alpha\rangle_L}{\partial x_i} - \frac{\partial M_j^\alpha}{\partial x_j} + \langle\omega_\alpha\rangle_L \tag{5}$$

where τ_{ij} is the viscous stress $T_{ij} = \langle u_i u_j\rangle_L - \langle u_i\rangle_L\langle u_j\rangle_L$ and $M_j^\alpha = \langle u_j\phi_\alpha\rangle_L - \langle u_j\rangle_L\langle\phi_\alpha\rangle_L$ denote the SGS stress and the SGS mass flux, respectively.

The closure problem in LES of non-reacting flows is essentially one of representing the unresolved terms T_{ij} and M_j^α in terms of the large, or the resolved scale variables. In reacting flows, the problem is compounded by the presence of the chemical source term, $\langle\omega_\alpha\rangle_L$, for which an additional model is required.

2.2 Hydrodynamic Closure

For closure of the hydrodynamic SGS stress, the gradient-diffusion approximation is invoked:

$$T_{ij} - (\delta_{ij}/3)T_{kk} = -2\nu_t\langle S_{ij}\rangle_L \tag{6}$$

where $\langle S_{ij}\rangle_L$ is the resolved strain rate tensor and ν_t is the SGS viscosity. The modified kinetic energy model (MKEV) is used to specify this viscosity[5]:

$$\nu_t = C_k\Delta_G\sqrt{|\langle u_i^*\rangle_L\langle u_i^*\rangle_L - \langle\langle u_i^*\rangle_L\rangle_{L'}\langle\langle u_i^*\rangle_L\rangle_{L'}|}, \tag{7}$$

where $u_i^* = u_i - U_i$ and U_i is a reference velocity in the x_i direction. The subscript L' denotes the filter at the secondary level which has a characteristic size (denoted by $\Delta_{G'}$) larger than that of grid level filter[2].

2.3 Scalar Closures

The gradient-diffusion approximation is also used for closure of the SGS mass fluxes[8]:

$$M_j^\alpha = -\Gamma_t\frac{\partial\langle\phi_\alpha\rangle_L}{\partial x_j} \tag{8}$$

where $\Gamma_t = \nu_t/Sc_t$, and Sc_t is the SGS Schmidt number and is assumed constant.

To take the effects of chemical reaction into account, we consider the transport of scalar array $\underline{\phi}(\underline{x},t) = [\phi_1,\phi_2,\ldots\phi_{N_s}]$ in a probabilistic manner. For that we use the "filtered density function" (FDF), denoted by f_L,[31]:

$$f_L(\underline{\psi};\underline{x},t) \equiv \int_{-\infty}^{+\infty}\varepsilon\left[\underline{\psi},\underline{\phi}(\underline{x}',t)\right]h_s(\underline{x}'-\underline{x})d\underline{x}', \tag{9}$$

$$\varepsilon\left[\underline{\psi},\underline{\phi}(\underline{x},t)\right] = \delta[\underline{\psi}-\underline{\phi}(\underline{x},t)] \equiv \prod_{\alpha=1}^{N_s}\delta[\psi_\alpha-\phi_\alpha(\underline{x},t)] \tag{10}$$

where δ denotes the delta function and $\underline{\psi}$ denotes the composition domain counterpart of the scalar vector $\underline{\phi}$. The term $\varepsilon[\underline{\phi} - \underline{\psi}(\underline{x},t)]$ is defined as the "fine-grained" density [25, 27], and Eq. (10) states that the FDF is the *spatially filtered* fine-grained density. Thus, f_L gives the density in the composition space of the fluid around $\underline{x}$ weighted by the filter h_ξ. Choosing a positive definite filter[34], ensures that f_L has all the properties of the PDF[30]. The FDF transport equation is derived by taking the time derivative of Eq. (9):

$$\frac{\partial f_L}{\partial t} + \frac{\partial \langle u_j \rangle_L f_L}{\partial x_j} = -\frac{\partial [\langle u_j | \underline{\psi} \rangle_L - \langle u_j \rangle_L] f_L}{\partial x_j} + \frac{\partial}{\partial \psi_\alpha} \left[\left\langle \frac{\partial J_j^\alpha}{\partial x_j} | \underline{\psi} \right\rangle_L f_L \right] - \frac{\partial [\widehat{S}_\alpha(\underline{\psi}) f_L]}{\partial \psi_\alpha}. \tag{11}$$

where $\widehat{S}_\alpha(\underline{\psi})$ is the composition domain representation of the source term, and the unclosed, conditionally filtered velocity is decomposed into its resolved and unresolved counterparts. This is an exact, transport equation for the FDF. The last term on the RHS is due to chemical reaction and is in a closed form. The second term on the left hand side represents the filtered convection of the FDF in physical space and is also closed (provided $\langle u_i \rangle_L$ is known). The unclosed terms are the first two terms on the RHS which represents the transport of the FDF via SGS convection, and the effects of diffusion in compositional space, due to molecular action. The SGS convective flux is modeled via the gradient-diffusion

$$[\langle u_j | \underline{\psi} \rangle_L - \langle u_j \rangle_L] f_L = -\Gamma_t \frac{\partial f_L}{\partial x_j}. \tag{12}$$

With the decomposition of the conditionally filtered velocity and the subsequent model (Eq. (12)) results similar to that in conventional LES for the first moment of the FDF are obtained:

$$\langle u_j \phi_\alpha \rangle_L = \langle u_j \rangle_L \langle \phi_\alpha \rangle_L + [\langle u_j \phi_\alpha \rangle_L - \langle u_j \rangle_L \langle \phi_\alpha \rangle_L], \tag{13}$$

$$[\langle u_j \phi_\alpha \rangle_L - \langle u_j \rangle_L \langle \phi_\alpha \rangle_L] = -\Gamma_t \frac{\partial \langle \phi_\alpha \rangle_L}{\partial x_j}. \tag{14}$$

The term in brackets in Eq. (13) is the generalized scalar flux in the form considered in conventional LES [16, 13]. Consequently, Eq. (14) becomes identical to Eq. (8).

The closure for the conditional SGS diffusion is based on the linear mean square estimation (LMSE) model [27, 7], which is also known as the interaction by exchange with the mean[3]. This is an entirely deterministic model and acts to relax the scalar values towards their ensemble mean. As input, the LMSE model requires the "frequency of mixing within the sub-grid," Ω_m, which is not known *a priori*. Analogous to the procedures in RANS, this frequency can be related to the SGS diffusion coefficient and the filter length: $\Omega_m = C_\Omega(\Gamma + \Gamma_t)/\Delta_G^2$. With these closures the modeled FDF transport equation is given by

$$\frac{\partial f_L}{\partial t} + \frac{\partial [\langle u_i \rangle_L f_L]}{\partial x_i} = \frac{\partial}{\partial x_i} \left[(\Gamma + \Gamma_t) \frac{\partial f_L}{\partial x_i} \right] + \frac{\partial}{\partial \psi_\alpha} [\Omega_m (\psi_\alpha - \langle \phi_\alpha \rangle_L) f_L] - \frac{\partial [\widehat{S}_\alpha(\underline{\psi}) f_L]}{\partial \psi_\alpha}. \tag{15}$$

This equation may be integrated to obtain transport equations for the SGS moments. The first moment, $\langle \phi_\alpha \rangle_L$, or the filtered mean is given by

$$\frac{\partial \langle \phi_\alpha \rangle_L}{\partial t} + \frac{\partial \langle u_i \rangle_L \langle \phi_\alpha \rangle_L}{\partial x_j} = \frac{\partial}{\partial x_j} \left[(\Gamma + \Gamma_t) \frac{\partial \langle \phi_\alpha \rangle_L}{\partial x_i} \right] + \langle \omega_\alpha \rangle_L. \tag{16}$$

3 NUMERICAL FORMULATION

The numerical solution of the hydro-scalar fields is a two step procedure. Utilizing a hybrid deterministic Eulerian hydrodynamic solver, and a stochastic Lagrangian species solver, the solution

proceeds in an explicit manner. The discretized equations are advanced in time until the desired time level is reached. Each time step consists of two parts. The first part is the advancement of the hydrodynamic equations, in the Eulerian reference frame. This is accomplished via high-order finite difference techniques. The second part is the advancement of the FDF. A Lagrangian Monte-Carlo technique is used for this purpose. Monte Carlo methods have been used with success in RANS calculations[30]. These methods involve the representation of the FDF with an ensemble of elements, distributed throughout the flow-field, from which the moments of interest may be calculated. There are two frameworks in which the elements are distributed: Eulerian and Lagrangian. In the Eulerian framework, elements are distributed at fixed nodes throughout the flow-field. The composition of these elements change due to the effects of convection, diffusion, mixing, and reaction. However, the number of the elements within a node and the location of the elements remain fixed[29]. In the Lagrangian framework, the elements are free to roam the physical domain as dictated by the hydrodynamic field, and the composition of the elements change only due to mixing and reaction.

Considering the spatial transport terms only, the FDF equation, Eq. (15), reduces to the Fokker-Planck, or Smoluchowski equation. The Fokker-Planck equation corresponds to the random diffusion process[14], represented by the stochastic differential equation (SDE)

$$dX_i(t) = D_i(\mathbf{X}(t),t)dt + E^{1/2}(\mathbf{X}(t),t)dW_i(t), \tag{17}$$

where X_i is the Lagrangian position, and W_i represents the Wiener-Lévy process[33]. Thus the spatial transport of the FDF is given by a Langevin equation The numerical implementation of the FDF consists of representing the FDF with a set of scalars $\phi_\alpha^{(n)}(\mathbf{X}^{(n)}(t),t)$ assigned on the particles throughout the flow-field. The location of the notional particles are given by $\mathbf{X}^{(\mathbf{n})}$. The numerical solution is facilitated via the Euler - Maruyamma integration scheme:

$$X_i^{(n)}(t_{k+1}) = X_i^{(n)}(t_k) + D_i^{(n)}(t_k)\Delta t + \left(E^{(n)}(t_k)\Delta t\right)^{1/2}\xi_i^{(n)}(t_k), \tag{18}$$

where $D_i^{(n)}(t_k) = D_i(\mathbf{X}^{(n)}(t_k),t)$, $E^{(n)}(t_k) = E(\mathbf{X}^{(n)}(t_k),t)$ and $\xi_i^{(n)}$ is a random variable with the standard Gaussian PDF. The coefficients D_i and E require the knowledge of the filtered mean velocity and the diffusivity. These are provided by the solution of Eqs. (3)-(4) by a finite difference LES then interpolated to the particle location. In obtaining these values, a 2nd order Lagrangian interpolation scheme is used. The scalar composition of each particle changes due to the effects of chemical reaction, and mixing, both of which are implemented deterministically.

4 RESULTS AND DISCUSSION

4.1 Numerical Specifications

Computations are performed on a domain of 14 jet exit diameters, (D), by 7 diameters by 3.5 diameters in the streamwise, cross-stream, and spanwise directions, respectively. The computational grid is evenly spaced, $\Delta_x = \Delta_y = \Delta_z = \Delta$, and is comprised of $101 \times 51 \times 25$ points. With this resolution, a Reynolds number of $Re_D = \frac{U_o D}{\nu} = 5,000$ is simulated, where ν is the kinematic viscosity. The value of the SGS viscosity constant is not optimized and is chosen to be $C_k = 0.015$. The grid filter size is taken to be $\Delta_G = 2\Delta$ and the ratio of the secondary filter width to that of the grid filter $\Delta_G{}'/\Delta_G$ is 3. The value of the molecular Schmidt and Prandtl numbers are chosen to be $Sc = Pr = 1$ and the SGS Schmidt and Prandtl numbers are chosen to be $Sc_t = Pr_t = 0.7$. In order to avoid large computational times, particles are clustered about the shear regions of the jet. This is the Lagrangian equivalent of grid clustering in Eulerian simulations. To preserve the statistics, each particle is given a weight which depends on the region of the flow into which it

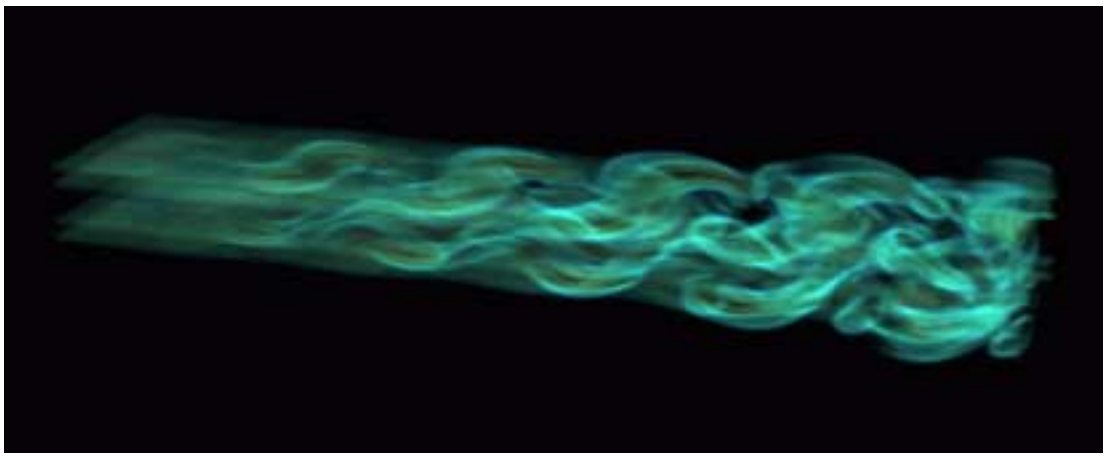

Fig. 1 Volume rendered vorticity magnitude.

is introduced. In evaluating the local value of the moments the particle weights are taken into account via:

$$\langle \phi \rangle_L = \frac{\sum_{i=1}^{N_p} \phi_i W_i}{\sum_{i=1}^{N_p} W_i}, \tag{19}$$

where W_i is the weight of the i-*th* particle, and N_p is the number of stochastic particles in the ensemble contained in volume $\Delta_V = {\Delta_E}^3$. Results are presented from the LES of three-dimensional (3D), planar jets under chemically reacting conditions. The configuration consists of a fluid issuing from jet slot of width D into a co-flowing stream. The space coordinates are $\mathbf{x} = [x, y, z]$, where x is the streamwise direction, y is the cross-stream direction and z is the spanwise direction. The velocity is initialized with a top-hat profile in the cross-stream direction, and is uniform in the spanwise direction. The initial speeds are U_o and U_∞ for the jet and the co-flowing stream, respectively. The velocity ratio is chosen to be $U_o/U_\infty = 2$. The jet contains species A and the co-flowing stream contains species B. Species A is initialized to be zero in the co-flowing streams and of unity mass fraction in the jet. Species B is initialized to be of unity mass fraction in the co-flowing streams and zero in the jet. In non-reacting flows species A, and B are conserved and passive scalars. In reacting flows, the species undergo a one-step, isothermal reaction of type $A + B \rightarrow P$. With these assumptions, the chemical source term is given by $\omega_A = \omega_B = -k_f Y_A Y_B$, where k_f is the reaction rate constant and Y_A, and Y_B denote the mass fractions of species A and B, respectively. The rate of chemical reaction is characterized by the Damköhler number, $Da = \frac{k_f D}{U_o}$. The limit $Da = 0$ corresponds to no reaction. Simulations are conducted in the infinite rate chemistry regime with $Da = 0.5$, and $Da = 2$. All species are assumed to have identical thermodynamic properties and the fluid is assumed to be a calorically perfect gas.

4.2 Non-reacting Flow

Simulations are conducted by (1) finite-difference, in which the SGS scalar-scalar interactions are neglected, and (2) the FDF methodology; Results obtained via the former are denoted LES-FD and results obtained via the latter are denoted FDF. A non-reacting simulation is performed in order to establish the consistency of the FDF methodology. That is, in the absence of chemical reaction, the results obtained by both methodologies should be similar. An instantaneous snapshot featuring the vorticity magnitude is shown in Fig. 1. This is accomplished using traditional raycasting techniques[23]. Rays are traced from the eye position through each pixel in the image plane and beyond, through the 3D data, to form a perspective projection of the dataset. Values at the evenly spaced grid points in the 3D vorticity magnitude volume are trilinearly interpolated to

evenly spaced sample locations along each viewing ray, shaded intensity and opacity values are computed at each sample point, a color wash is applied, and the results are composited in front-to-back order. The color and opacity mappings are defined to highlight roughly 33% of the peak value. The 3D coherent structures are evident as the fluid rolls up and begin to pair[4]. Figure

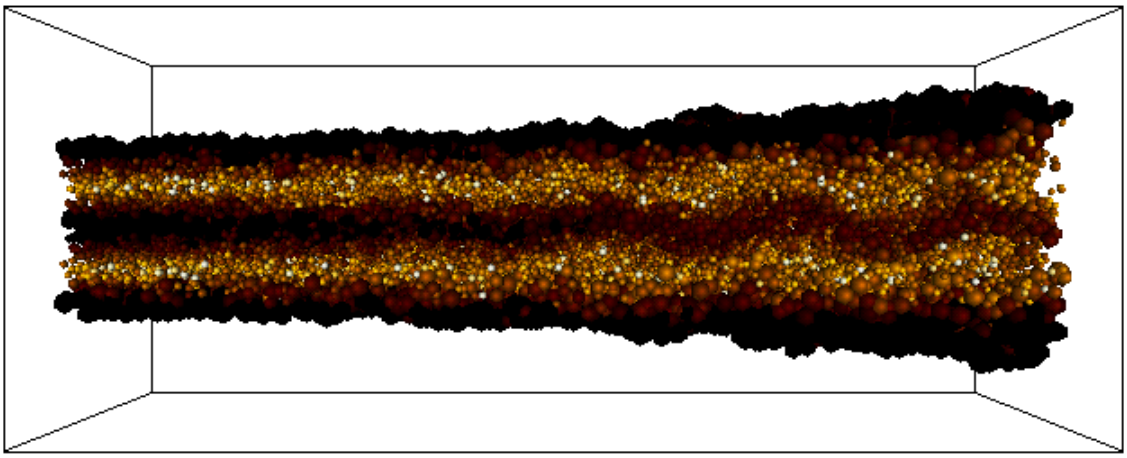

Fig. 2 Monte Carlo particles.

2 portrays the spatial distribution of the Monte Carlo particle at one instant in time. The particle number density ranges from 100 in the free stream to over 300 in the shear and core regions of the jet, with a total of roughly $1,400,000$ particles throughout the domain (for purposes of clarity only 2% of the particles illustrated). This is sufficient to keep statistical errors in predicting the scalar moments at sufficiently low levels. Fewer particles are placed in the free-stream region of the flow where no chemical reaction is anticipated. These particles are accordingly are "heavier." The consistency of the methodology is established by considering the scatter plot of the instantaneous means predicted by both methodologies shown in Fig. 3a. A linear regression analysis performed on the instantaneous, filtered, scalar mean yields a correlation coefficient of 0.99 and a slope of 1.

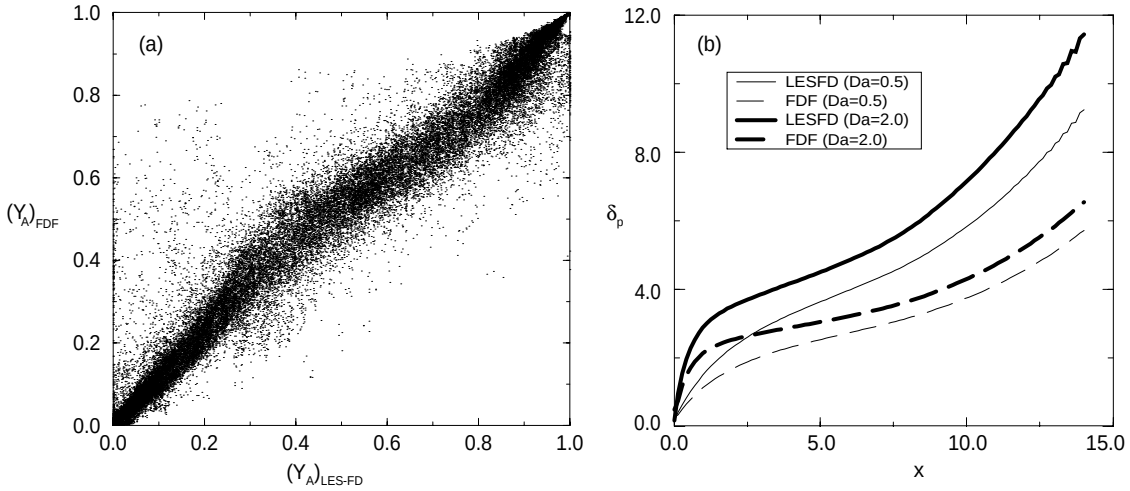

Fig. 3 Predicted mass fractions: (a) conserved scalar, Y_A, $Da = 0$; (b) time-averaged product thickness.

4.3 Reacting Flows

The results for reacting flows can be summarized by Fig. 3b which shows the integrated total product - $\delta_P(x) = \int_{-\infty}^{\infty}\int_{-\infty}^{\infty}\overline{\langle Y_P\rangle}_L(x,y,z)dydz$ throughout the domain. This reveals that LES-FD over-predicts the rate of reactant conversion in comparison to the FDF. In addition, it shows that, as the Damköhler number increases, the discrepancy between the two methodologies also increases. The LES-FD over predicts the FDF by as much as 60% and 80% at $Da = 0.5$, and $Da = 2.0$, respectively. This reveals that unresolved scalar correlations play a significant role at higher reaction rates. Figure 4 shows the volume rendered, instantaneous, product mass fraction as predicted by both the LES-FD and the FDF. We use a moment-value-to-opacity mapping that favors the display of voxels whose values are in the vicinity of the target iso-surface but does not strictly preclude the visibility of voxels of other, more distant values. This allows us to visualize each of the surfaces within the slightly larger global context of the entire 3D moment distribution. To facilitate comparison, we used identical value-to-color and opacity mappings in the rendering of each dataset. Because the mean of the values in the FDF distribution was smaller than the mean of the values in the LES-FD distribution it was difficult to define a single mapping function that showed each volume to its greatest advantage. It is evident that in addition to a higher rate of reactant conversion, the LES-FD calculation yields a 3D spatial structure which is very different in comparison to the FDF.

4.4 Extraction and Visualization of Dynamic Features

One of the greatest challenges that we face in visualizing the results of these simulations is posed by the sheer quantity of data produced. A typical three-dimensional DNS of turbulent flow may require a computational mesh consisting of $800 \times 400 \times 200$ grid points. Such a calculation will produce $1.6GB$ of data at each time step. However only a fraction of the data produced at each time step, the data that indicates the location of the iso-surface, is of final interest; the remainder only provides the global context that supports the evolution of the simulation. Current practice, which is to save the data over the full grid at every 100 time steps, is straightforward but extraordinarily inefficient. We are currently exploring alternative approaches to saving the data, in which only the specific subportions of the volume that are necessary for reconstructing the location of the flame surface are written out to disk. However there are many challenges in saving the data in a form that allows easy reconstruction of the pertinent information without excessive overhead. For example, when the data is saved across an entire uniform grid, one needs only a 6 byte header to store the dimensions of the grid, in addition to the 4 bytes per grid point required to store the actual data. The potential exists to save both time and space by recording the data only at a select subset of the grid points; however the locations of these grid points must then also be explicitly recorded, requiring a 6 byte overhead per point. In tests conducted on a 150 second FDF simulation, it was found that, on average, data at only 4% of the grid points at each time

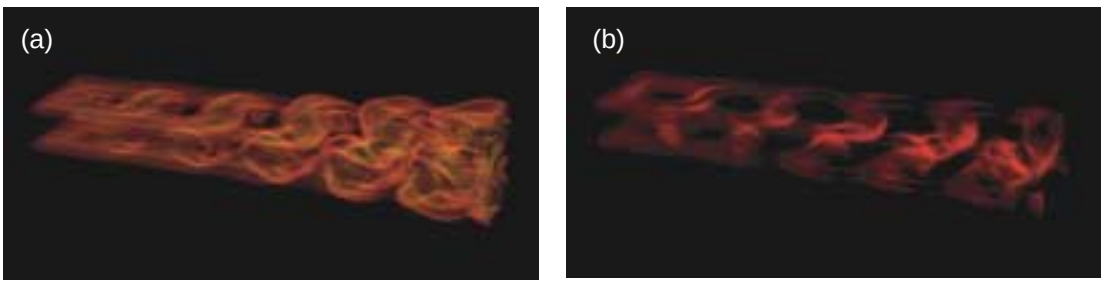

Fig. 4 Instantaneous, volume rendered product mass fraction, Y_P : (a) LES-FD; (b) FDF.

step were critical to the reconstruction of the flame surface. For a similar LES-FD simulation over the same grid, data at an average of 15% of the grid points was pertinent. By recording only the necessary minimum of data values, space savings of over 90% could be achieved for the FDF data using this approach. In the case of the LES-FD simulation, where the number of relevant grid points exceeds 8% of the total, it becomes more efficient rather than to record the locations of the points on an individual basis, to use a binary map to encode the occupancy of the full grid. Space savings of 76% and 74% was achieved in the LES-FD and FDF simulations, respectively, using this method. Combined, these techniques facilitate the visualization of large three-dimensional datasets. Figure 5 portrays both the iso-surface defined by $Y_p = 0.5$, and the volume rendered vorticity magnitude. Such representation helps to elucidate the nature of the underlying hydrochemical interactions.

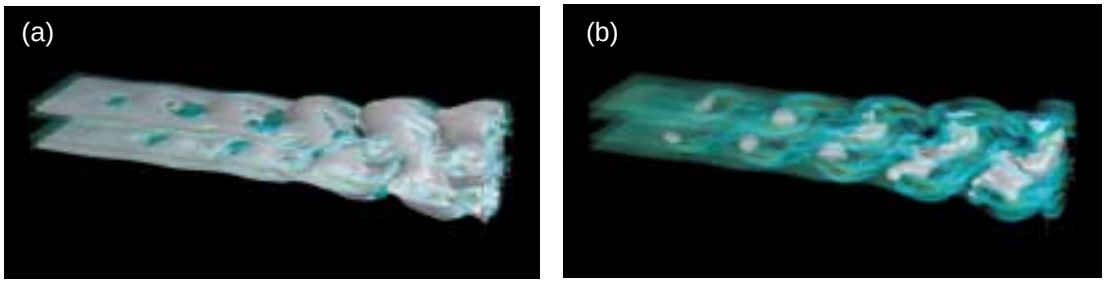

Fig. 5 Three-dimensional hydroscalar structure: (a) LES-FD; (b) FDF.

5 ACKNOWLEDGEMENTS

This work is supported by the National Science Foundation under Grant ACI-9982274. Computational resources are provided by the Minnesota Supercomputing Institute.

REFERENCES

[1] Aldama A. A. Filtering techniques for turbulent flow simulations. Vol. 49, New York, NY, 1990. Springer-Verlag.

[2] Bardina J, Ferziger J. H, and Reynolds W. C. Improved turbulence models based on large eddy simulations of homogeneous, incompressible, turbulent flows. Department of Mechanical Engineering Report TF-19, Stanford University, Stanford, CA, 1983.

[3] Borghi R. Turbulent combustion modeling. *Prog. Energy Combust. Sci.*, Vol. 14, pp 245–292, 1988.

[4] Brown G. L and Roshko A. On density effects and large structure in turbulent mixing layers. *J. Fluid Mech.*, Vol. 64, pp 775–816, 1974.

[5] Colucci P. J, Jaberi F. A, Givi P, and Pope S. B. Filtered density function for large eddy simulation of turbulent reacting flows. *Phys. Fluids*, Vol. 10, No 2, pp 499–515, 1998.

[6] Cook A. W and Riley J. J. A subgrid model for equilibrium chemistry in turbulent flows. *Phys. Fluids*, Vol. 6, No 8, pp 2868–2870, 1994.

[7] Dopazo C and O'Brien E. E. Statistical treatment of non-isothermal chemical reactions in turbulence. *Combust. Sci. and Tech.*, Vol. 13, pp 99–112, 1976.

[8] Eidson T. M. Numerical simulation of the turbulent Rayleigh-Benard problem using subgrid modelling. *J. Fluid Mech.*, Vol. 158, pp 245–268, 1985.

[9] Ferziger J. H. Higher level simulations of turbulent flows. Stanford University Report TF-16, Department of Mechanical Engineering, Stanford University, Stanford, CA, 1981.

[10] Ferziger J. H. Large eddy simulations: Its role in turbulence research. In Dwoyer D. L, Hussaini

M. Y, and Voigt R. G, editors, *Theoretical Approaches in Turbulence*, pp 51–72, New York, NY, 1987. Springer-Verlag.

[11] Ferziger J. H and Peric M. *Computational Methods for Fluid Dynamics*. Springer-Verlag, New York, NY, 1996.

[12] Frankel S. H, Adumitroaie V, Madnia C. K, and Givi P. Large eddy simulations of turbulent reacting flows by assumed PDF methods. In Ragab S. A and Piomelli U, editors, *Engineering Applications of Large Eddy Simulations*, pp 81–101, New York, NY, 1993. ASME, FED-Vol. 162.

[13] Gao F and O'Brien E. E. A large-eddy simulation scheme for turbulent reacting flows. *Phys. Fluids A*, Vol. 5, No 6, pp 1282–1284, 1993.

[14] Gardiner C. W. *Handbook of Stochastic Methods: for Physics, Chemistry and the Natural Sciences*. Springer, New York, NY, 1985.

[15] Garrick S. C, Jaberi F. A, and Givi P. Large eddy simulation of scalar transport in a turbulent jet flow. In Knight and Sakell [21], pp 155–166.

[16] Germano M. Turbulence: The filtering approach. *J. Fluid Mech.*, Vol. 238, pp 325–336, 1992.

[17] Givi P. Spectral and random vortex methods in turbulent reacting flows. In Libby P. A and Williams F. A, editors, *Turbulent Reacting Flows*, pp 475–572, London, UK, 1994. Academic Press.

[18] Hill J. C. Homogeneous turbulent mixing with chemical reaction. *Ann. Rev. Fluid Mech.*, Vol. 8, pp 135–161, 1976.

[19] Jaberi F. A, Colucci P. J, James S, Givi P, and Pope S. B. Filtered mass density function for large eddy simulation of turbulent reacting flows. *J. Fluid Mech.*, 1999.

[20] Jones W. P and Whitelaw J. H. Calculation methods for reacting turbulent flows: A review. *Combust. Flame*, Vol. 48, pp 1–26, 1982.

[21] Knight D and Sakell L. Vol. 54 of *Fluid Mechanics and its Applications*, Kluwer Academic Publishers, The Netherlands, 1999.

[22] Kollmann W, editor. *Prediction Methods for Turbulent Flows*. Hemisphere Publishing Co., New York, NY, 1980.

[23] Levoy M. Display of surfaces from volume data. *IEEE Comp Graphics and App.*, Vol. 8, No 3, pp 29–37, 1988.

[24] Libby P. A and Williams F. A, editors. *Turbulent Reacting Flows*. Vol. 44 of *Topics in Applied Physics*, Springer-Verlag, Heidelberg, 1980.

[25] Lundgren T. S. Distribution functions in the statistical theory of turbulence. *Phys. Fluids*, Vol. 10, No 5, pp 969–975, 1967.

[26] Madnia C. K and Givi P. Direct numerical simulation and large eddy simulation of reacting homogeneous turbulence. In Galperin B and Orszag S. A, editors, *Large Eddy Simulations of Complex Engineering and Geophysical Flows*, pp 315–346, Cambridge, UK, 1993. Cambridge University Press.

[27] O'Brien E. E. The probability density function (PDF) approach to reacting turbulent flows. In Libby and Williams [24], chapter 5, pp 185–218.

[28] Pope S. B. The statistical theory of turbulent flames. *Phil. Trans. Royal Soc. London*, Vol. 291, No 1384, pp 529–568, 1979.

[29] Pope S. B. A Monte Carlo method for the PDF equations of turbulent reactive flow. *Combust. Sci. and Tech.*, Vol. 25, pp 159–174, 1981.

[30] Pope S. B. PDF methods for turbulent reactive flows. *Prog. Energy Combust. Sci.*, Vol. 11, pp 119–192, 1985.

[31] Pope S. B. Computations of turbulent combustion: Progress and challenges. *Proceedings of 23rd Symp. (Int.) on Combustion*, pp 591–612, Pittsburgh, PA, 1990. The Combustion Institute.

[32] Reynolds O. On the dynamical theory of incompressible viscous fluids and the determination of the criterion. *Phil. Trans. Royal Soc.*, Vol. 123, 1895.

[33] Risken H. *The Fokker-Planck Equation, Methods of Solution and Applications*. Springer-Verlag, New York, NY, 1989.

[34] Vreman B, Geurts B, and Kuerten H. Realizability conditions for the turbulent stress tensor in large-eddy simulation. *J. Fluid Mech.*, Vol. 278, pp 351–362, 1994.